

# Combining ferromagnetic resonator and digital image correlation to study the strain induced resonance tunability in magnetoelectric heterostructures

Fatih Zighem<sup>1,\*</sup>, Mohamed Belmeguenai<sup>1</sup>, Damien Faurie<sup>1,†</sup>, Halim Haddadi<sup>2</sup>, and Johan Moulin<sup>3</sup>

<sup>1</sup>*Laboratoire des Sciences des Procédés et des Matériaux,  
CNRS-Université Paris XIII, Sorbonne Paris Cité, Villetaneuse, France*

<sup>2</sup>*Laboratoire MSMP—Carnot Arts, ENSAM ParisTech,  
rue Saint-Dominique, 51006 Châlons-en-Champagne, France and*

<sup>3</sup>*Institut d'Electronique Fondamentale, UMR 8622, Université Paris Sud-CNRS, Orsay, France*

(Dated: July 28 2014)

This paper reports the development of a methodology combining microstrip ferromagnetic resonance (MS-FMR) and digital image correlation (DIC) in order to simultaneously measure the voltage-induced strains and the magnetic resonance in artificial magnetoelectric heterostructures (“magnetic films/piezoelectric substrate” or “magnetic films/flexible substrate/piezoelectric actuator”). The overall principle of the technique and the related analytical modelling are described. It is powerful to estimate the magnetostriction coefficient of ferromagnetic thin films and can be used to determine the effective magnetoelectric coefficient of the whole heterostructures in addition to the piezoelectric coefficient related to the in-plane voltage-induced strains. This methodology can be applied to system for which the strains are well transmitted at the different interfaces.

PACS numbers:

Keywords: indirect magnetoelectric effect, digital image correlation, ferromagnetic resonance

## I. INTRODUCTION

During the last decade, many groups have concentrated their effort on the study of ferromagnetic resonance (FMR) tunability through electric field strain induced MagnetoElectric (ME) coupling [1, 2]. Many ME systems based on ferromagnetic/ferroelectric heterostructures have been developed, encompassing voltage-tunable microwave signal processing devices [3–5], magnetoelectric random access memory devices [6–9] and strain-control GMR devices [10–12]. For all these kinds of systems, the properties are controlled *via* the elastic voltage-induced strains transmitted from the ferroelectric medium to the ferromagnetic one. Hence, the knowledge of the elastic strains must be known in order to predict the changes of magnetic state induced by applying voltages. Concerning magnetic thin films deposited on substrates, there are two ways to control the magnetization by applying voltage-induced strains : i) deposition of the film on a piezoelectric substrate [13–15] and ii) deposition of the film on a “non-piezoelectric” substrate and subsequent cementation on a piezoelectric actuator [16–18]. In the first one, the in-plane strain transmission is generally good, the main disadvantage being to transfer existing process to piezoelectric substrates (PZT, PZN-PT, PMN-PT, ...) ; in the second one, the main problem is the possibly bad in-plane strain transmission when the substrate is rigid (Si, GaAs, MgO, ...), the total transmission being attained only with compliant substrates (polymers) [19]. In the

two cases of full transmission (“film/piezoelectric substrate”, “film/polymer substrate/piezoelectric actuator”), the knowledge of the in-plane strains in the piezoelectric substrate or actuator is sufficient to know the in-plane strains in the whole system. In order to measure simultaneously the in-plane strains and ferromagnetic resonance in such systems, we have developed a methodology combining *in situ* microstrip ferromagnetic resonance (MS-FMR) with the Digital Image Correlation (DIC) technique. In this paper, we will show the general principle of the technique including the analytical formalism, before describing the experimental details. Then we will show an example of study on a “Finemet® film/Kapton® substrate/piezoelectric actuator” system highlighting the potentialities of the method. Especially, we will show that this technique is very efficient to determine the magnetostriction coefficient at saturation of the film, in complement to recently developed techniques for thin films, such as magnetoelastic measurement setup with a MOKE magnetometer [20], substrate deflection method under magnetic field [21], laser Doppler vibrometry [22], applied whole wafer curvature [23], strain modulated ferromagnetic resonance [24], or vibrating sample magnetometer coupled with bending [25].

## II. PRINCIPLE

### A. Methodology

The voltage strain-induced magnetoelectric coupling in artificial multiferroic systems, consisting on a magnetic film deposited onto a piezoelectric substrate, is based on a two step process: i) the application of an electric field inside the piezoelectric medium induces mechani-

\*Electronic address: zighem@univ-paris13.fr

†Electronic address: faurie@univ-paris13.fr

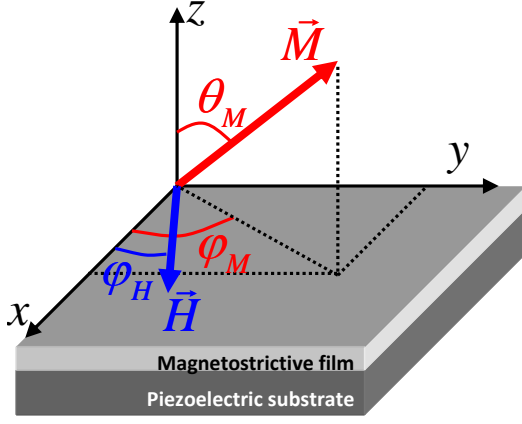


Figure 1: Schematic illustration showing angles, fields and coordinate systems used in the text.

cal deformations to the magnetic film *via* piezoelectric effect and ii) magnetostriction of the magnetic film induces a magnetoelastic anisotropy which can be strain(or voltage)-tuned in amplitude and direction. In these conditions, a quantitative evaluation of this indirect magnetoelectric coupling requires both the determination of the strains induced by the piezoelectric medium to the ferromagnetic film and the induced magnetoelastic anisotropy. These parameters can be evaluated with our experimental setup. Indeed, with our setup, when applying a voltage to the piezoelectric medium, it is possible to simultaneously measure the induced mechanical deformation and the magnetoelastic anisotropy thanks to a combination of digital image correlation and broadband ferromagnetic resonance techniques. Indeed, the uniform precession mode resonance field is directly linked to the magnetoelastic anisotropy when the film is submitted to external stresses. In these conditions, it is not only possible to measure an effective magnetoelectric coupling which do not necessary require the strains evaluation inside the magnetic film but also the magnetostriction coefficients. The following paragraph presents a basic analytical modelling of the resonance field variation as function of external applied stresses.

## B. Theoretical background

In this paragraph, the resonance field of the uniform precession mode of a magnetostrictive film submitted to in-plane external stresses is derived in the macrospin approximation (*i. e.* a uniform magnetization is considered). In our system, these in-plane stresses are applied by the piezoelectric medium to the ferromagnetic film (see figure 1). For simplicity, the magnetostrictive and elastic properties of this thin film are considered as isotropic (it will be the case in the studied system). With these assumptions (isotropic behavior and macrospin approximation), the magnetostriction coefficient,

the Young's modulus and the Poisson's ratio of the thin film are scalar parameters. The magnetic energy of the thin film, using the coordinates system presented in Figure 1 can be written as:

$$F = F_{zee} + F_{dip} + F_{me} \quad (1)$$

Where the two first terms stand for the Zeeman and the dipolar contributions, respectively. The last term corresponds to the magnetoelastic anisotropy term and can be written as:

$$F_{me} = -\frac{3}{2}\lambda \left( \left( \cos^2 \varphi_M \sin^2 \theta_M - \frac{1}{3} \right) \sigma_{xx} + \left( \sin^2 \varphi_M \sin^2 \theta_M - \frac{1}{3} \right) \sigma_{yy} \right) \quad (2)$$

$\sigma_{xx}$  and  $\sigma_{yy}$  being the in-plane principal stress tensor components while  $\theta_M$  and  $\varphi_M$  stand for the polar and the azimuthal angles of the magnetization  $\vec{M}$ . Finally,  $\lambda$  is the isotropic magnetostriction coefficient at saturation of the thin film. The relation between the principal stress components ( $\sigma_{xx}$ ,  $\sigma_{yy}$ ) and strains ( $\varepsilon_{xx}$ ,  $\varepsilon_{yy}$ ) tensors is given by the isotropic Hook's law where  $E$  is the Young's modulus and  $\nu$  is the Poisson's ratio:

$$\sigma_{xx} = \left( \frac{E}{1+\nu} \right) \left( \frac{1}{1-\nu} \varepsilon_{xx} + \frac{\nu}{1-\nu} \varepsilon_{yy} \right) \quad (3)$$

$$\sigma_{yy} = \left( \frac{E}{1+\nu} \right) \left( \frac{1}{1-\nu} \varepsilon_{yy} + \frac{\nu}{1-\nu} \varepsilon_{xx} \right) \quad (4)$$

The resonance field of the uniform precession mode evaluated at the equilibrium is obtained from the following expression:

$$\left( \frac{2\pi f}{\gamma} \right)^2 = \left( \frac{1}{M_s \sin \theta_M} \right)^2 \left( \frac{\partial^2 F}{\partial \theta_M^2} \frac{\partial^2 F}{\partial \varphi_M^2} - \left( \frac{\partial^2 F}{\partial \theta_M \partial \varphi_M} \right)^2 \right) \quad (5)$$

Where  $f$  is the microwave driving frequency and  $\gamma$  is the gyromagnetic factor ( $\gamma = g \times 8.794 \times 10^6 \text{ s}^{-1} \cdot \text{Oe}^{-1}$ ). The different energy derivatives are evaluated for the equilibrium direction of the magnetization. For an in-plane applied magnetic field, the equilibrium polar angle is  $\varphi_M = \frac{\pi}{2}$  because of the large effective demagnetizing field associated with the planar film geometry and an explicit expression is obtained:

$$\begin{aligned} \left( \frac{2\pi f}{\gamma} \right)^2 = & \left[ 4\pi M_s + H_{res} \cos(\varphi_M - \varphi_H) + \right. \\ & \left. \frac{3\lambda}{M_s} \left( \sigma_{xx} \cos^2 \varphi_M + \sigma_{yy} \sin^2 \varphi_M \right) \right] \times \\ & \left[ H_{res} \cos(\varphi_M - \varphi_H) + \frac{3\lambda}{M_s} \left( \sigma_{xx} \cos^2 \varphi_M + \sigma_{yy} \sin^2 \varphi_M \right) \right] \quad (6) \end{aligned}$$

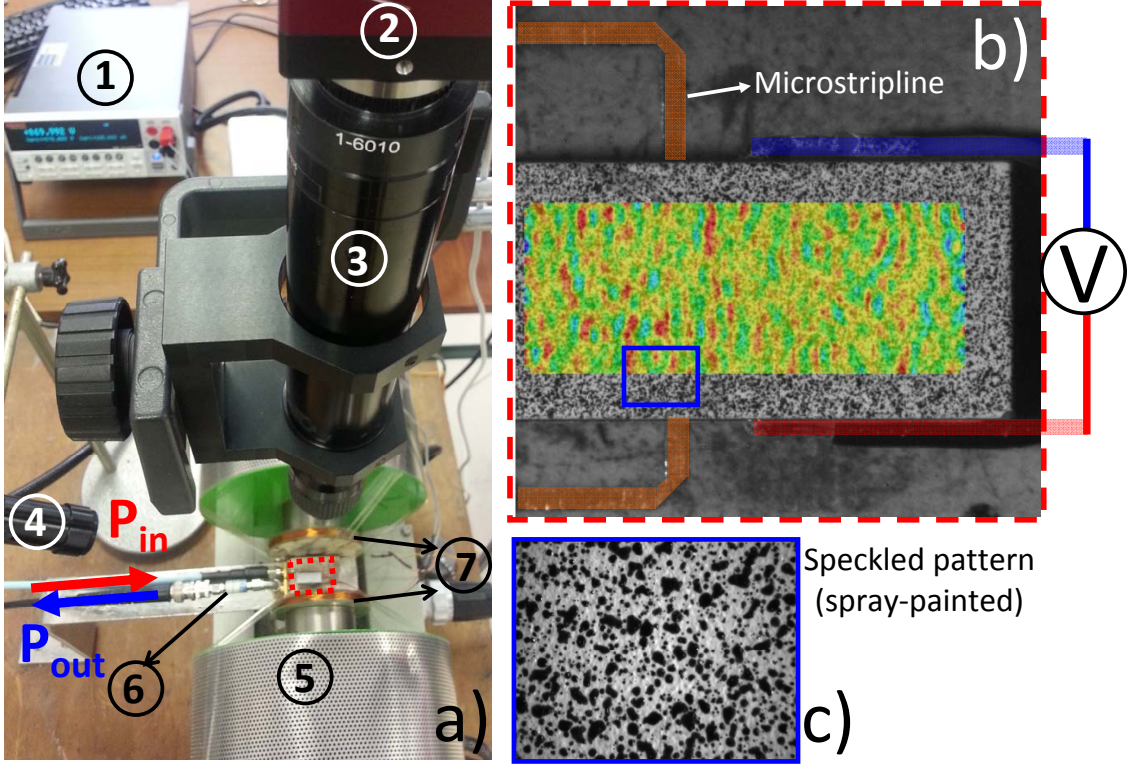


Figure 2: a) Setup image of the combined MS-FMR/DIC experiment. The circled numbers correspond to: ①: Keithley Model 2400; ②: CCD camera (AVT-Pike-f421b); ③: objective lens for the CCD camera; ④: white light source; ⑤: electromagnet; ⑥: Schottky detector and ⑦: modulation coils.  $P_{in}$  and  $P_{out}$  are the injected and transmitted radio frequency current. b) Zoom in showing the sample mounted onto the microstripline. A typical calculated strain field map is present at the top of the sample. c) Zoom in of the speckled pattern (spray-painted) at the top of the sample necessary for the strain fields calculations.

Here  $\varphi_H$  is the angle between the in-plane applied magnetic field and  $x$  direction (see figure 1). The analysis can be simplified if the resonance field is larger than the magnetoelastic anisotropy field ( $\vec{H}_{me} = -\vec{\nabla}_M F_{me}$ ). In this condition, the magnetization direction is almost aligned along the applied magnetic field ( $\varphi_M \sim \varphi_H$ ). The resonance field is thus given by:

$$H_{res} = \sqrt{\left(2\pi M_s + \frac{3\lambda}{2M_s}(\sigma_{xx} \sin^2 \varphi_H + \sigma_{yy} \cos^2 \varphi_H)\right)^2 + \left(\frac{2\pi f}{\gamma}\right)^2} - 2\pi M_s - \frac{3\lambda}{4M_s}(\sigma_{xx}(1+3\cos 2\varphi_H) + \sigma_{yy}(1-3\cos 2\varphi_H)) \quad (7)$$

The two first terms represents an almost constant shift in the resonance field baseline because  $2\pi M_s$  and  $\frac{2\pi f}{\gamma}$  are found to be larger than the magnetoelastic and the magnetoelastic anisotropy field. The last term correspond to the angular variation of the resonance field due to the voltage induced magnetoelastic anisotropy field.

### III. EXPERIMENTAL SETUP

The experimental setup presented in figure 2 has been developed in order to *in situ* study the indirect magnetoelectric effect occurring in artificial magnetoelectric multiferroics heterostructures such as the ones presented in introduction. Our setup combines microstrip ferromagnetic resonance (MS-FMR) and digital image correlation (DIC) techniques. The MS-FMR characterization is performed with the help of a field modulated FMR setup using HP 83752B generator, operating in the 0.01-20 GHz frequency range, to generate a radio frequency field ( $\vec{h}_{rf}$ ) of variable power (-100 dBm to +20 dBm). The sample (figure 2b)) is mounted on a 0.5 mm microstrip line (the film side is in direct contact with the microstripline) connected to the HP generator *via* a semi-flexible SMA cable and to a lock-in amplifier (Stanford research system SR830) to derive the field modulated measurements *via* a Schottky detector. The microstrip line (MS), composed of 0.5 mm Cu-strip grown on Cu-back side metalized  $\text{Al}_2\text{O}_3$  substrate, is designed to have 50 Ohm characteristic impedance and broadband. The MS and the sample are inserted inside the gap of an electromagnet connected to a DC power supplier to generate in-plane

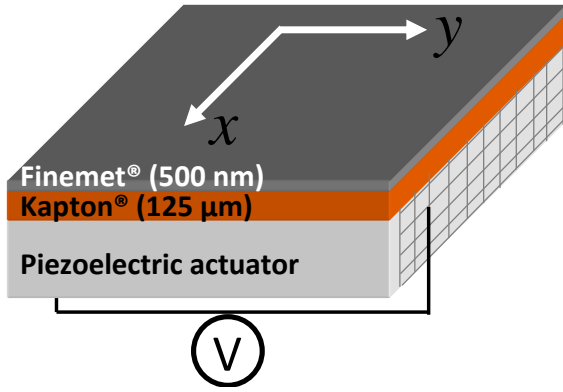


Figure 3: Sketch of the studied heterostructure showing the 500 nm thick Finemet® film deposited onto a 125  $\mu\text{m}$  thick Kapton® substrate and glued onto the piezoelectric actuator.

magnetic fields up to 5 kOe with a resolution of 0.1 Oe. This external magnetic field is modulated at a frequency of 170 Hz with an amplitude varying from 1 to 8 Oe allowing lock-in detection to be used in order to increase the signal-to-noise ratio. This broadband MS-FMR offers a high sensitivity allowing to detect a net magnetic moment down to  $10^{-5}$  emu.

The piezoelectric media is connected to a Keithley power supplier (Model 2400) allowing to apply DC voltages in the range  $[-200 \text{ V}; +200 \text{ V}]$  with 0.001 V resolution. For each applied voltage, a MS-FMR spectrum and an image of the top surface of the sample are recorded (note that the spectrum recording takes from 1 minutes to several hours depending on the magnetic field step and on the total width of the spectrum). The images recording at each step will serve to determine the in-plane field strains. Furthermore, being given the initial “homogeneous” surface of the sample, a speckle pattern has been spray painted in order to generate a contrast which will serve to calculate the strain fields (an image of a typical speckled pattern (spray-painted) is presented in Figure 2c)). In our setup, the images are recorded thanks to a  $2048 \times 2048$  pixels CCD AVT-Pike f421b camera vertically positioned in the top of the surface sample. The objective lens has been chosen in order to be sufficiently far from the electromagnet (20 cm) with a field view around  $1 \times 1 \text{ cm}^2$  as shown on Figure 2b). The strain fields calculations (from the different images) have been performed by digital image correlation. Several commercial and open source softwares based on digital image correlation technique are available (Ncorr [26], Moire [27], Aramis [28], Matchid [29], Correli [30], ...) for the determination of strains fields. In the following illustrative results, the DIC calculations have been performed by using Aramis. Finally, it is worth to mention that this setup is piloted *via* a Labview program providing flexibility of a real time control of the magnetic field and the DC voltage sweeps, step and rate, real time data acquisition and visualization.

#### IV. ILLUSTRATIVE RESULTS

The methodology is illustrated with a “magnetic film/polymer substrate/piezoelectric actuator” system. Figure 3 presents a cross-section sketch of the fabricated heterostructure. An amorphous 530 nm thick Finemet® film has been deposited onto a 125  $\mu\text{m}$  thick polyimide flexible substrate (Kapton®) by radio frequency sputtering. The deposition conditions were a residual pressure of around  $10^{-7}$  mbar, a working Ar pressure of 40 mbar and a RF power of 250 W. Prior to the Finemet® deposition, a 10 nm thick Ti buffer layer, was deposited on the substrate to ensure a proper adhesion of the Finemet® film. Finally, another 10 nm thick Ti cap layer was deposited on the top of the Finemet® film in order to protect it from oxidation. The composition of the film has been measured by EDS (Energy Dispersive Spectroscopy) and is close to that of the target ( $\text{Fe}_{73.5}\text{Cu}_1\text{Nb}_3\text{Si}_{15.5}\text{B}_7$ ) while the thickness of the film (530 nm) has been measured by Scanning Electron Microscopy. After deposition, the film/substrate system has been glued onto a piezoelectric actuator.

The figure 4 shows the map of the in-plane strains ( $\varepsilon_{xx}$ ,  $\varepsilon_{yy}$ ,  $\varepsilon_{xy}$ ) for a few voltages applied to the piezoelectric actuator (from 0 V to +150 V). For the three in-plane strain components, the whole distribution is estimated to be about  $10^{-4}$  so that the strain heterogeneities in the piezoelectric actuator are relatively weak. Obviously, to interpret the FMR results, we use the mean values of the elastic strains. When we apply a voltage, the mean values of  $\varepsilon_{xx}$  and  $\varepsilon_{yy}$  vary with  $\frac{\varepsilon_{yy}}{\varepsilon_{xx}} \sim -0.65$ , while the in-plane shear strain  $\varepsilon_{xy}$  remains unchanged. This behavior is illustrated in figures 5-a and 5-b where the mean strains  $\varepsilon_{xx}$  and  $\varepsilon_{yy}$  are plotted as function of the voltage.

In 5-a, the curve corresponds to a simple electric loading-unloading (0V - 150V - 0V) ; the non-linearity of the curve is due to the specific piezoelectric behavior of the actuator, which is reversible. In figure 5-b, we show an unloading from 150V to -150V and a subsequent loading from -150V to 150V. We observe the so-called “butterfly” behavior that is due to polarization switching at about -60V during unloading and 60V during loading. In addition, we have checked that the analysis of  $\varepsilon_{xx}$  and  $\varepsilon_{yy}$  on the thin film gives same mean values[19]. Thus, the transmission of the in-plane strains between the actuator and the surface of the film is close to 100%.

The voltage induced anisotropy has been studied in a specific configuration (magnetic field  $\vec{H}$  applied along  $y$  axis). The influence of the applied voltage on the magnetic properties of the thin film has been probed by MS-FMR technique. Figures 5-c and 5-d show MS-FMR results obtained from experimental spectra recorded at 8 GHz with an applied magnetic field along the  $y$  axis (*i.e.*  $\varphi_H = \frac{\pi}{2}$ ) and for different applied voltages; typical experimental spectra are shown on figure 6-a. In these conditions, the deduced resonance fields are in a magnetic saturating regime so that we can deduce here the magnetostriction coefficient at saturation. It clearly appears



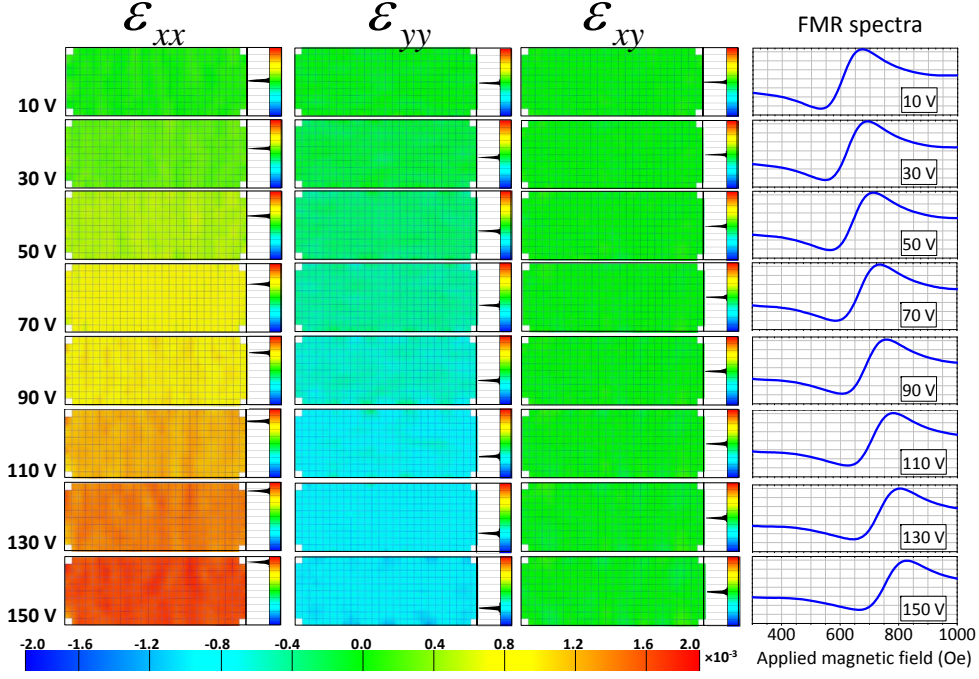


Figure 4: Calculated in-plane strains fields ( $\varepsilon_{xx}$ ,  $\varepsilon_{yy}$  and  $\varepsilon_{xy}$ ) and corresponding FMR spectra for specific applied voltages (from 0 V to +150 V). Histograms of the in-plane strains fields are represented for each applied voltage. Note the almost zero value of the shear strain ( $\varepsilon_{xy}$ ).

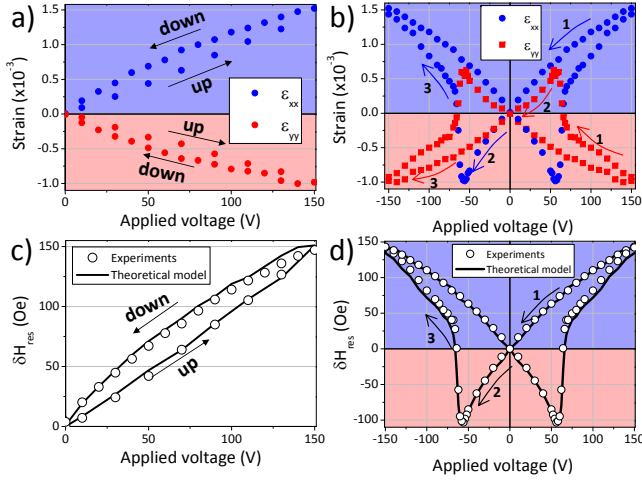


Figure 5: Mean in-plane strains ( $\varepsilon_{xx}$  and  $\varepsilon_{yy}$ ) and  $\delta H_{res}$  variations as function of the applied voltage (a,c: from 0 to +150 V and back to 0 V; b,d: from +150 V to -150 V and back to +150 V). The continuous lines in c) and d) are calculated by using equation 7 with the following parameters:  $\gamma = 1.885 \times 10^7 \text{ s}^{-1} \cdot \text{Oe}^{-1}$ ,  $M_S = 965 \text{ emu} \cdot \text{cm}^{-3}$ ,  $E = 145 \text{ GPa}$  and  $\nu = 0.27$  and  $\lambda = 17.5 \times 10^{-6}$ .

that the resonance field increases with the applied voltage, which indicates that the  $y$  axis is harder and the  $x$  axis easier for the magnetization direction when a positive voltage is applied. This is consistent with a positive

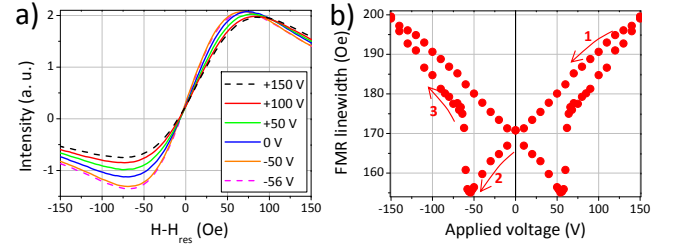


Figure 6: a) Typical FMR spectra obtained at 8 GHz showing the linewidth variation as function of the applied voltage. For clarity, they are centered around 0 Oe (shifted by their respective resonance field). b) Corresponding FMR linewidth ( $\Delta H_{pp}$ ) variation as function of the applied voltage (from +150 V to -150 V and back to +150 V).

magnetostriction coefficient, as expected for amorphous Finemet® alloys [31]. The shift of the resonance fields as function of the applied voltage are presented in figures 5-c and 5-d and corresponds to the tests shown respectively in figures 5-a and 5-b for the strain analysis. Obviously, the observed non-linear and hysteretic variations of the resonance field is due to the variations of  $\varepsilon_{xx}$  and  $\varepsilon_{yy}$  as function of the applied voltage (see figure 3). In order to quantitatively bind the resonance field variations to the in-plane strains induced by the applied voltage, we can calculate the uniform precession mode frequency as function of the applied voltage (strain) by

adding a magnetoelastic energy term  $F_{me}$  to the total magnetic energy density  $F$  of the film, as described previously. The solid lines in Figures 5-c and 5-d are fits to the experimental data calculated by using the parameters previously determined by MS-FMR ( $\gamma = 1.885 \times 10^7 \text{ s}^{-1} \cdot \text{Oe}^{-1}$ ,  $M_S = 965 \text{ emu} \cdot \text{cm}^{-3}$ ) and Brillouin light scattering ( $E = 145 \text{ GPa}$  and  $\nu = 0.27$ ) [32]. Actually, the magnetostriction coefficient of the thin film is the sole parameter to be determined using this experiment and has been estimated to be  $\lambda = 17.5 \times 10^{-6}$ , slightly lower than the bulk counterpart ( $\lambda = 23 \times 10^{-6}$ ) [31].

In addition, in figure 6-b, the FMR peak to peak linewidth ( $\Delta H_{pp}$ ), defined as the field difference between the extrema of the sweep-field measured FMR spectra, is plotted as function of the applied voltage using 8 GHz driving frequency. This figure shows that  $\Delta H_{pp}$  is significantly enhanced by the applied voltage and interestingly presents similar behavior as the resonance field shift and the strain (5-b and 5-d) suggesting its correlation with the voltage induced strain. The modelling of the strain behavior of the FMR linewidth is out of this paper scope and will be addressed in forthcoming papers. However, this strain tuning of the FMR linewidth remains a simple and promising manner to artificially choose the desired damping depending on the aimed application.

## V. CONCLUSION AND PERSPECTIVES

We have shown a methodology that combines microstrip ferromagnetic resonance (MS-FMR) and digital

image correlation (DIC) in order to study the voltage-induced strains effect on magnetic anisotropy in thin films. The elastic strains are measured on the actuator (or substrate) side while the magnetic resonance field is measured in the thin films. This technique allows determining the magnetostriction coefficient of the film and can also be used to determine the effective magnetoelectric coefficient of the whole system and the piezoelectric coefficient related to the in-plane voltage-induced strains. This methodology can be applied to system for which the strains are well transmitted at the different interfaces (“film/piezoelectric substrate” system or “film/polymer substrate/piezoelectric actuator” system). Moreover, the strain tuning of the FMR linewidth is promising for spintronics applications. Indeed, the magnetic damping controls how fast the magnetization reverses and therefore is interesting technological parameter.

## Acknowledgments

The authors gratefully acknowledge the CNRS for his financial support through the “PEPS INSIS” program (FERROFLEX project) and the Université Paris 13 through a “Bonus Qualité Recherche”.

- 
- [1] Y. K. Fetisov and G. Srinivasan, Appl. Phys. Lett. Appl. Phys. Lett. **88**, 143503 (2006)
  - [2] G. Srinivasan, Ann. Rev. Mater. Res. **40**, 153-178 (2010)
  - [3] G. Subramanyam, M. W. Cole, N. X. Sun, Thottam S. Kalkur, N. M. Sbrockey, G. S. Tompa, X. Guo, C. Chen, S. P. Alpay, G. A. Rossetti Jr., K. Dayal, L.-Q. Chen and D. G. Schlom, J. Appl. Phys. **114**, 191301 (2013)
  - [4] M. Liu, Z. Zhou, T. Nan, B. M. Howe, G. J. Brown and N. X. Sun, Adv. Mater. **25**, 1435-1439 (2013)
  - [5] I. V. Zavislyak, M. A. Popov, G. Sreenivasulu and G. Srinivasan, Appl. Phys. Lett. **102**, 222407 (2013)
  - [6] T. X. Nan, Z. Y. Zhou, J. Lou, M. Liu, X. Yang, Y. Gao, S. Rand, and N. X. Sun, Appl. Phys. Lett. **100**, 132409 (2012)
  - [7] Y. T. Yang, Y. Q. Song, D. H. Wang, J. L. Gao, L. Y. Lv, Q. Q. Cao and Y. W. Du, J. Appl. Phys. **115**, 024903 (2014)
  - [8] S. Fusil, V. Garcia, A. Barthelémy, M. Bibes, Ann. Rev. Mater. Res. *in press*, DOI: 10.1146/annurev-matsci-070813-113315 (2014)
  - [9] T. Jin, L. Hao, J. Cao, M. Liu, H. Dang, Y. W., D. Wu, J. Bai, and F. Wei, Appl. Phys. Expr. **7**, 043002 (2014)
  - [10] S. Rizwan, S. Zhang, T. Yu, Y. G. Zhao and X. F. Han, J. Appl. Phys. **113**, 023911 (2013)
  - [11] M. Liu, S. Li, O. Obi, J. Lou, S. Rand and N. X. Sun, Appl. Phys. Lett. **98**, 222509 (2011)
  - [12] N. Lei, T. Devolder, G. Agnus, P. Aubert, L. Daniel, J.-V. Kim, W. Zhao, T. Trypiniotis, R. P. Cowburn, C. Chappert, D. Ravelosona and P. Lecoeur, Nature Com. **4**, 1378 (2013)
  - [13] C. Thiele, K. Dörr, O. Bilani, J. Rödel, L. Schultz, Phys. Rev. B **75**, 054408 (2007)
  - [14] J. H. Park, J.-H. Lee, M. G. Kim, Y. K. Jeong, M.-A. Oak, H. M. Jang, H. J. Choi, and J. F. Scott, Phys. Rev. B **81**, 134401 (2010)
  - [15] D. A. Filippov, G. Srinivasan and A. Gupta, J. Phys. Cond. Matter **20**, 425206 (2008)
  - [16] C. Pettiford, J. Lou, L. Russell, and N. X. Sun, App. Phys. Lett. **92**, 122506 (2008)
  - [17] C. Bihler, M. Althammer, A. Brandlmaier, S. Geprägs, M. Weiler, M. Opel, W. Schoch, W. Limmer, R. Gross, M. S. Brandt and S. T. B. Goennenwein, Phys. Rev. B **78**, 045203 (2008)
  - [18] A. Brandlmaier, S. Geprägs, M. Weiler, A. Boger, M. Opel, H. Huebl, C. Bihler, M. S. Brandt, B. Botters, D. Grundler, R. Gross and S. T. B. Goennenwein, Phys. Rev. B **77**, 104445 (2008)
  - [19] F. Zighem, D. Faurie, S. Mercone, M. Belmeguenai and H. Haddadi, J. App. Phys. **114**, 073902 (2013)
  - [20] I. G. Will, A. Ding, and Y. B. Xu, Rev. Sci. Instr. **83**,

- 064707 (2012)
- [21] W. Brückner, C. Lang and C. M. Schneider, *Rev. Sci. Instr.* **72**, 2496 (2001)
  - [22] R. Varghesea, R. Viswanb, K. Joshia, S. Seifikarc, Y. Zhoua, J. Schwartzc, S. Priyaa, *J. Mag. Mag. Mater.* **363**, 179–187 (2014)
  - [23] C. B. Hill, W. R. Hendren, R. M. Bowman, P. K. McGeehin, M. A. Gubbins and V. A. Venugopal, *Meas. Sci. Tech.* **24**, 045601 (2013)
  - [24] K. Nesteruk, R. Żuberek, S. Piechota, M. W. Gutowski and H. Szymczak, *Meas. Sci. Tech.* **25**, 075502 (2014)
  - [25] B. Buford, P. Daghat and A. Jander, *J. Appl. Phys.* **115**, 17E309 (2014)
  - [26] <http://www.ncorr.com/>
  - [27] <http://www.opticist.org/>
  - [28] <http://www.gom.com/>
  - [29] <http://www.matchid.org/>
  - [30] G. Besnard, F. Hild, S. Roux, *Exp Mech* **46**, 789 (2006).
  - [31] J. Moulin, I. Shahosseini, F. Alves, F. Mazaleytrat, *Journal of Micromechanics and Microengineering* **21**, 074010 (2011)
  - [32] A. Fillon, C. Jaouen, A. Michel, G. Abadías, C. Thomas, L. Belliard, B. Perrin, P. Djemia, *Phys. Rev. B* **88**, 174104 (2014)